An Investigation of the Effect of Varied Blade Shapes of the Trim Interceptor on the Resistance Characteristics of a Planing Vessel at Medium Speeds

Dimas Fajar Prasetyo[1], Rina Rina[1], Muhammad Luqman Hakim[1,2,*], Dian Purnama Sari[1], Muryadin Muryadin[1], Nanang Setiyobudi[1,3], Endah Suwarni[1], Putri Virliani[1], Nurcholis Nurcholis[1], Fariz Maulana[1], Shinta Johar Alif Rahadi[1], Yuniati Yuniati[1]

[1] Research Center for Hydrodynamics Technology, National Research and Innovation Agency (BRIN), Surabaya 60117, Indonesia
[2] Department of Naval Architecture, Faculty of Engineering, Universitas Diponegoro, Semarang 50275, Indonesia
[3] Department of Marine Engineering, Institut Teknologi Sepuluh Nopember, Surabaya, 60111, Indonesia

ARTICLE INFO	ABSTRACT
  	The use of trim interceptors on fast boats to enhance performance still presents challenges in achieving optimal design across various parameters. The design of interceptor blades with conventional square cross-sections prompts consideration of whether altering the blade shape can affect its effectiveness in minimizing resistance on planing boats. This comprehensive study explores various permutations of interceptor blade shapes and their impact on the characteristics of resistance in planing botas. Computational Fluid Dynamics (CFD) using the Reynolds Averaging Navier-Stokes (RANS) method, verified and validated, is employed to conduct this investigation. The results indicate that the round shape consistently exhibits lower resistance compared to rectangular, ½ V, and full V shapes across a range of speeds (Froude number 0.76 – 0.99).

1. Introduction

High-speed craft, the ships or boats capable of traveling at high speeds, require a greater amount of energy compared to regular ships. Fast boats have a higher energy consumption-to-payload ratio compared to regular ships or those not classified as fast boats. These boats are intentionally designed to travel swiftly, much like airplanes focused on delivering passengers or cargo quickly. Similarly, high-speed vehicles like sports cars utilize engines much larger than other components [1]. This design logic makes sense because as speed increases, energy requirements increase even more. The drag force on a boat increases proportionally with the square of its speed (V^2), while power increases proportionally with the cube of its speed (V^3) [2]. Therefore, it is clear that higher speeds pose the risk of increased energy consumption. Thus, a slight reduction in resistance can be beneficial in

---

* *Corresponding author.*
E-mail address: mluqmanhak@lecturer.undip.ac.id (Muhammad Luqman Hakim)

reducing emissions. Although small in amount, if all fast boats reduce their emissions slightly, it will cumulatively have a significant impact on reducing global emissions.

Several efforts can be made to reduce emissions or decrease energy consumption by minimizing the drag force on ships, including for the fast boats. For instance, slight modifications to the hull shape can enhance overall performance, such as opting for a U or V-shaped hull [3], employing steps in hull design, either single step or double steps [4, 5], or utilizing added waterjet intake plane shapes [6]. Additionally, maintaining hull performance to prevent disturbances from biofouling can also prevent energy wastage [7–11]. Another effective method is the installation of additional devices on the hull [12], such as trim interceptors [13, 14], trim tabs [15, 16], stern foils [17], spray strips [18], [19], and chine strips [20], which can also enhance the performance of fast boats.

The effectiveness of trim interceptors on fast boats still encounters numerous challenges stemming from various parameters of both the boat hull and the interceptor design itself, including the shape of the interceptor blade. Trim interceptors are typically installed on the transom, as illustrated in Fig. **1**. Their primary role is to modify local flow and generate lift force, thereby reducing trim angle and drag force [14]. Karimi *et al.,* [21] further support this by noting a reduction in resistance of up to 15% for monohull models and up to 12% for catamaran models. However, Samuel *et al.,* [13] emphasize that the effectiveness of interceptors relies heavily on their dimensions and positions; incorrect dimensions and placement may actually increase drag. Additionally, the hull shape design, such as deadrise angle, also influences the effectiveness of interceptor usage [22]. Furthermore, the selection of speed (Froude number) plays a significant role; interceptors prove most beneficial in reducing resistance at Fr 0.7-0.1 [13]. The shape of the trim interceptor blade is another crucial factor that impacts its effectiveness in enhancing the performance of fast boats.
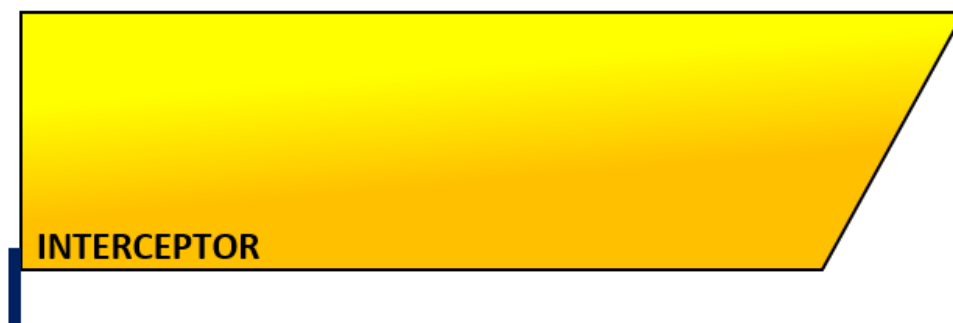
Fig. 1. Utilization of interceptors on high-speed planing boats

Research on the influence of interceptor blade cross-sectional shape is currently limited. Typically, interceptor blades are flat with a certain thickness, featuring rectangular cross-sections. From these rectangular shapes, there is potential to modify them into other shapes, such as triangular or rounded. Therefore, investigation is needed to determine whether modifying the cross-sectional shape of interceptor blades can enhance their effectiveness.

This study aims to investigate the impact of different cross-sectional shapes of interceptor blades on the resistance values of fast vessels. The methodology employed requires a numerical approach utilizing multi-fluid RANS-CFD (the Reynolds Averaging Navier-Stokes Computational Fluid Dynamics) methods. The object used for installing the interceptor is a patrol boat that has been constructed and is operational. The investigated data includes total resistance values, frictional resistance, and residual resistance. It is expected that the results of this research will contribute to furthering the understanding of interceptors and enhancing the performance of fast boats.

2. Methodology
2.1 Research Object and Variation

The research focuses on a model scale of a fast patrol boat as its study subject—a vessel that has been successfully constructed and is currently operational. The characteristics of this boat are detailed in Table 1, accompanied by a three-dimensional illustration in Fig. **2**. This vessel serves as a practical and tangible object of study, offering real-world insights into the application of the research findings.

Table 1
The planing boat general parameters, full scale and model scale

Data	Vessel	Model
Length, LOA (m)	17.08	2.995
Length, LWL (m)	15.923	2.7915
Length, LPP (m)	`	2.7376
Breadth, B (m)	4	0.7011
Height, H (m)	2.25	0.3945
Draft, T (m)	0.7	0.1227
Displacement (kg)	20806.47	108.95
Scale	1 : 1	1 : 5.704
Deadrise angle (degree)	15	15
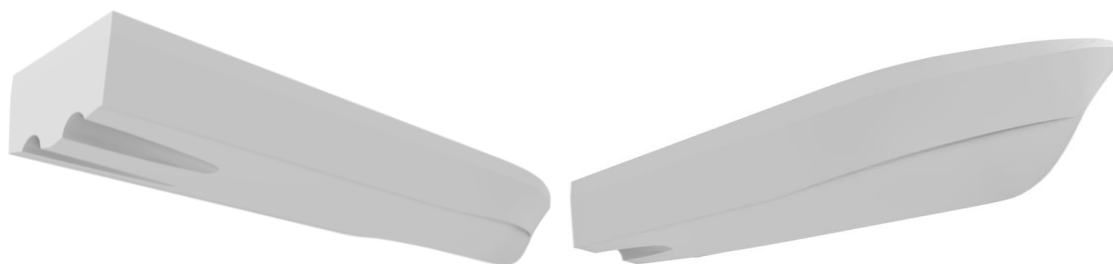
Fig. 2. Three-dimensional illustration of the vessel as the object research

The primary focus of variation in this research lies in the diverse cross-sectional shapes of the interceptor blades. The interceptor's design is divided into four segments, as depicted in Fig. **3** and Fig. **4**. Previous research conducted by Jangam [23] has indicated that the optimal height of the interceptor should range between 1% and 2.5% of the stern's width, potentially resulting in a reduction in resistance by 6% to 14%. This analysis provides the dimensions of the square-shaped (original) blade, detailed in Table 2 and Fig. **3**. Subsequently, the interceptor blade is modified to include the ½ V, Round, and Full-V designs, with the dimensions of each shape provided in Table 3. Fig. **4** visually presents the modified blade interceptors on the stern side. All blades maintain a consistent total height of 10 mm, which is 2.5% of B (hull width).
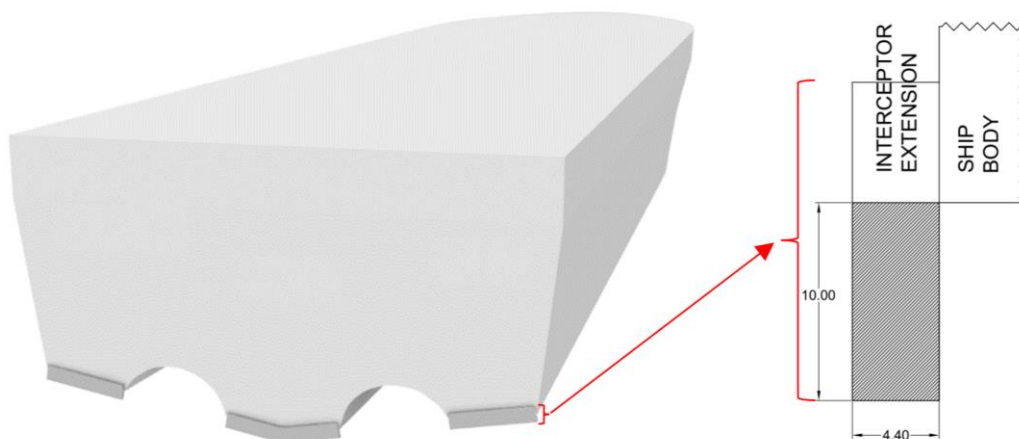
Fig. 3. Illustration depicting the installation of the original (square) interceptor with dimensions specified in millimeter

Table 2
The square-shaped (original) interceptor blade dimensions

Data	Model	Vessel
Height (mm)	10	57.0
Width (mm)	4.4	25.1
Length	Alongside stern transom	Alongside stern transom

Table 3
The varied sectional shaped of the interceptor blade dimensions

Tip Model	Total Height (mm)	Width (mm)	Slope (mm)	Diameter (mm)
Triangle-shape (**1/2 V**)	10	4.4	6.66	-
Half Sphere-shape (**round**)	10	4.4	-	4.4
V-shape (**full V**)	10	4.4	5.46	-
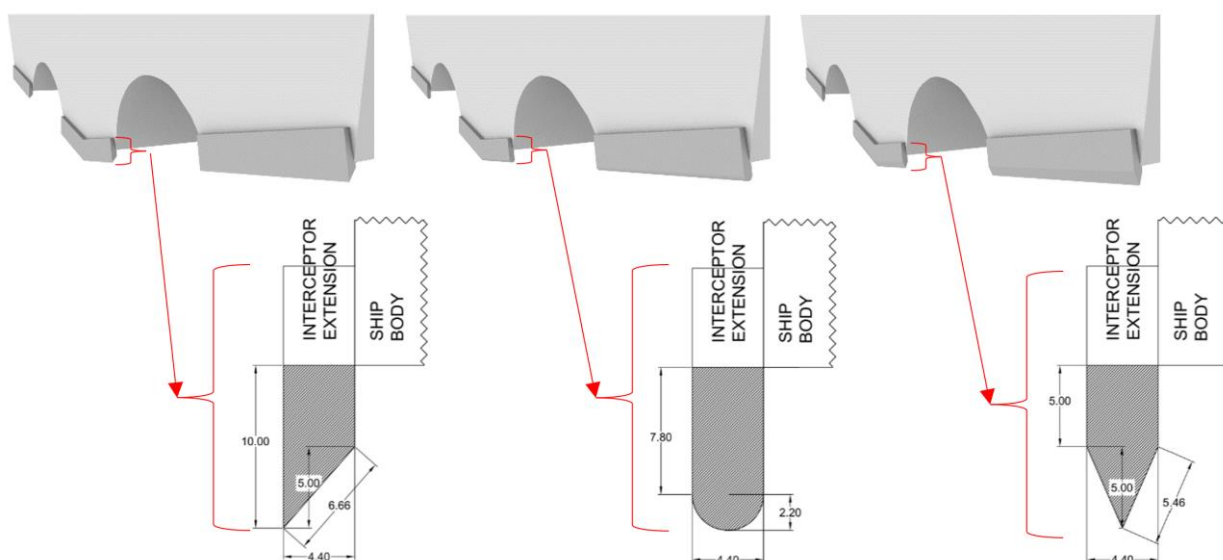
Fig. 4. Illustration of variations in the cross-sectional shape of interceptor blades, from left to right: ½ V, Round, and Full-V shapes in millimeters

2.2 CFD Set Up
2.2.1 Governing equation

The prediction results for this investigation were obtained by Computational Fluid Dynamics (CFD) simulations using governing equations from unstable Reynolds-Averaged Navier-Stokes (uRANS) simulations. It was thought that the fluid in question was incompressible and had Newtonian properties. A constant viscosity throughout the fluid is implied by the Newtonian fluid assumption [24]. On the other hand, homogeneous fluid density during the simulation is required in order to take into account incompressibility. Eq. (1) and Eq. (2) present the average continuity and momentum equations, respectively. In these equations, U_i represents the average speed component, $\bar{P}$ stands for the average pressure, ρ signifies the effective density of the fluid, μ denotes the effective viscosity, u_i' represents the fluctuation velocity component, $\rho\overline{U_i'U_j'}$ represents the Reynolds stress, and $\overline{\tau_{ij}}$ is the tensor component of the mean viscous stress [25], as detailed in Eq. (3).

$$\frac{\partial(\rho\overline{U_i})}{\partial x_i} = 0 \tag{1}$$

$$\frac{\partial(\rho\overline{U_i})}{\partial t} + \frac{\partial}{\partial x_i}\left(\rho\overline{U_i}\overline{U_j} + \rho\overline{U_i'U_j'}\right) = -\frac{\partial\bar{P}}{\partial x_i} + \frac{\partial\overline{\tau_{ij}}}{\partial x_j} \tag{2}$$

$$\overline{\tau_{ij}} = \mu\left(\frac{\partial\overline{U_i}}{\partial x_j} + \frac{\partial\overline{U_j}}{\partial x_i}\right) \tag{3}$$

The volume fraction feature used to define the water and air fluid regions in the computer model is defined by Eq. (4). The Volume of Fluid (VOF) technique was used in this simulation because it is effective at representing discrete flow phases. The designated computational domain, denoted by V, encompasses volume of fluid 1 (V_1) and volume of fluid 2 (V_2). Using the method recommended by Hirt and Nichols [26], assigning a volume fraction value of 1 or 0 to every grid cell allows for a clear separation of the water and air fluids.

$$\alpha(\vec{x}, t) = \begin{cases} \Delta_1, \vec{x}, \in V_1 \\ \Delta_0, \vec{x}, \in V_2 \end{cases} \tag{4}$$

The volume fraction's continuity equations seek to express how each component in a mixture's mass is conserved. These continuity equations for individual phases find expression in Eq. (5) and Eq. (6) in the context of two-phase flow. Within these Equations, α_1 and α_2 denote the volume fractions of the first and second fluids, respectively; ρ_1 and ρ_2 represent the densities of the first and second fluids, respectively $\overline{U}$ corresponds to the boat's speed; and ∇ signifies the divergence operator. The VOF C_{ijk} function is an integral of $\alpha(\vec{x}, t)$ on each grid cell in every volume cell, as detailed in Eq. (7), which is subsequently expressed as Eq. (8). In this context, $C = 1$ signifies the grid defining the fluid, whereas $C = 0$ indicates that the grid comprises a mixture of water and air phases, specifically under the air phase when $0 < C < 1$.

$$\frac{\partial(\alpha_1\rho_1)}{\partial t} + \overline{U} \cdot \nabla(\alpha_1\rho_1) = 0 \tag{5}$$

$$\frac{\partial(\alpha_2\rho_2)}{\partial t} + \overline{U} \cdot \nabla(\alpha_2\rho_2) = 0 \tag{6}$$

$$C_{ijk} = \frac{1}{\Delta V_{ijk}} \int \alpha(\vec{x}, t) dV \qquad (7)$$

$$\frac{\partial C}{\partial t} + \bar{U} \cdot \nabla C = 0 \qquad (8)$$

For this investigation, the SST (Shear Stress Transport) k-ω model of turbulence was used. Specifically designed for accurate modelling at the wall region, this model incorporates the k-ω wall function, which captures the features of turbulent flow. Moreover, the model integrates the k-ε model, which is appropriate for simulating the flow domain's far field. Combining these two models into the SST k-ω model guarantees a thorough description of turbulence across the flow field [27].

Because it directly affects the Courant number, choosing the right time step value is crucial in simulations that are prone to instability. The International Towing Tank Conference (ITTC) suggests a time step in the range of $\Delta t = 0.005 - 0.01 L/V$, where V is the boat velocity and L is the hull length, in order to guarantee reliable results [28]. Following this advice, the simulation running now uses a time step value that is within the recommended range, which guarantees the accuracy of the findings. Maintaining numerical stability and faithfully representing transitory phenomena in the simulation need careful consideration of the time step.

2.2.2 Boundary conditions and mesh generation

Based on the recommendations of the International Towing Tank Conference (ITTC) regarding the computational domain, specific guidelines must be adhered to. The distance from the bow of the front vessel to the inlet boundary should be equal to one vessel length (L), and similarly, the distance from the transom to the outlet boundary should be four vessel lengths (4L). The keel to bottom boundary distance should be two vessel lengths (2L), while the hull side to the wall boundary distance should also be one vessel length (L) [28], see Fig. **5**.

ITTC further specifies the minimum number of cells for CFD analysis, with the cell at the wall determined by y^+. The targeted y+ value is around 50, where the recommendation is 30< y+ < 300 [28]. The analysis utilizes approximately 1,359,253 cells. Fig. **5** illustrates the simulation domain and mesh density configuration for the upcoming simulation. The RANS equation assumes that ship speed and size demonstrate turbulence effects on the hull. The simulations employ the $k - \omega$ model to represent turbulence impact on flow near walls [27]. Ensuring convergence in simulations requires reducing RMS error values to 10^{-4} or 10^{-5}. Boundary conditions will be defined with gravity for top and bottom boundaries, while others will be set to far field. Detailed boundary settings are provided in Table 4.

Using two degrees of freedom—free heave and trim—dynamic mesh was used to mimic boat motion using dynamic fluid-body interaction (DFBI). The study used an overset grid system and the motion of a rigid body to show how the boat moved in the fluid realm. Eq. (9) and Eq. (10), respectively, provided the basis for simulating translational (sinkage) and rotational (trim) motions at the boat model's centre of mass [13, 29]. These equations involve various variables: M, representing the net moment acting on the boat model for y-axis rotation; I, the moment of inertia for y-axis rotation; ω, the angular velocity of the boat for y-axis rotation; m, the mass of the boat; F, the net force acting on the surface of the boat for z-axis translation; and U, the speed of the boat. Forces and moments acting on the boat were derived from fluid pressure and shear forces on the boat's surface.

$$I \frac{d\omega}{dt} = \sum M \tag{9}$$

$$m \frac{dU}{dt} = \sum F \tag{10}$$

(a)   (b)
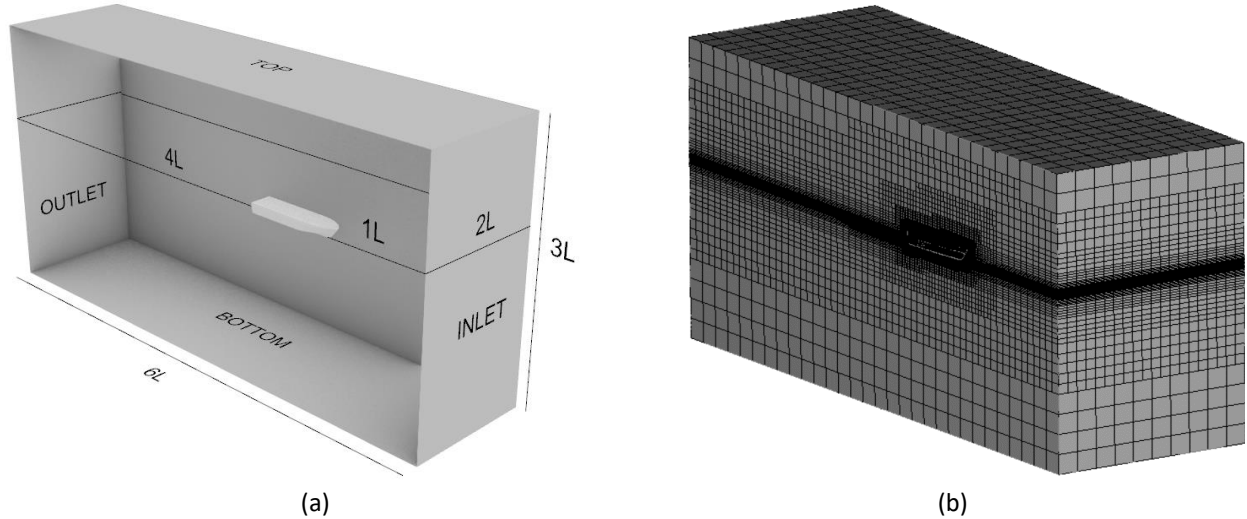
Fig. 5. (a) Domain for computation (b) grid density

Table 4
Boundary conditions setting up

Surface	Boundary condition
Xmax, Inlet (EXT)	Far Field
Xmin, Outlet (EXT)	Far Field
Ymax, Side (Ext)	Far Field
Ymin, Mirror (MIR)	Far Field
Zmax, Top (EXT)	Prescribed Pressure
Zmin, Bottom (EXT)	Prescribed Pressure
Surface, DECK (SOL)	No Slip
Surface, OTHERS (SOL)	Wall

3. Results and Discussions
3.1 Verification and Validation

This segment looks at the simulation's uncertainty values to determine how sensitive numerical computations are to discretization error or cell count. The results of the verification test with different numbers of meshes are shown in Table 5 and shown in Fig. **6**. Eq. (11) is used to calculate the percentage difference in simulation results caused by an increase in mesh count. Given the available computational resources, a mesh with a medium configuration (1.35 million) will be regularly employed for the future simulations. As a result, given the verification test findings, the numerical uncertainty value stays below 0.42%.

Table 5
Simulation results depicting variations in the number of meshes and their numerical uncertainty

Configuration (n)	Number of cells (in millions)	R_T (N)	ε
1 (coarse)	0.65	131.61	
2 (coarse-medium)	0.970	127.04	-3.47%
3 (medium)	1.35	124.81	-1.76%
4 (medium-fine)	1.680	124.72	-0.07%
5 (fine)	2.11	124.28	-0.35%

$$\varepsilon = \frac{\left| R_{T_{(n+1)}} - R_{T_{(n)}} \right|}{R_{T_{(n)}}} \times 100\% \tag{11}$$
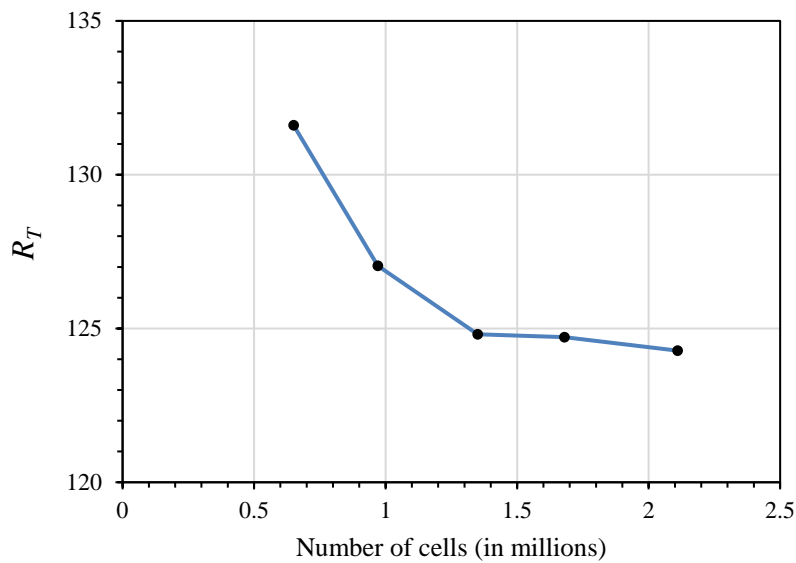
Fig. 6. Convergence curve for the independence test of the number of cells for verification numerical uncertainty

An essential part of this work is validation analysis, which comprises a careful comparison of the results from the present Computational Fluid Dynamics (CFD) simulation with the experimental data and empirical calculation. Fig. **7** provides a clear visualisation of the curve that represents the initial comparison evaluation. Eq. (12), which gives the prediction error in relation to the experiment, is utilised to further elucidate the consistency of the data. To improve the thoroughness of the validation procedure, a third comparison study employing the Root Mean Square of Error (RMSE) methodology is conducted, as indicated by Eq. (13). The authors claim that significant insights have been obtained from this validation exercise based on the completed comparison results. Fig. **7** visual analysis shows that the curves are quite near to one another, suggesting that the outcomes are quite comparable. The Root Mean Square of Error (RMSE) is roughly 3.27% when all error values are used in the computation. Generally speaking, the comparatively low RMSE value in this instance indicates that CFD simulations generally agree well with the reference experimental data.
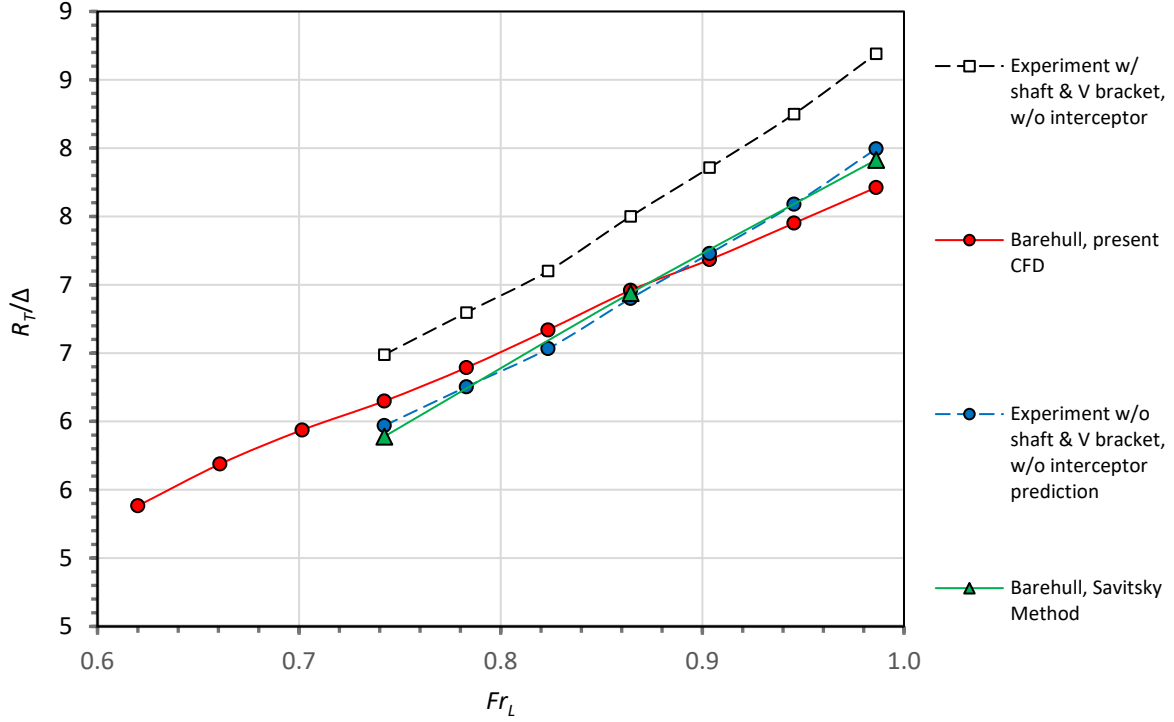
Fig. 7. This CFD simulation's results are compared to experimental and empirical results as a validation

$$E_\% = \frac{\left(\frac{R_{T(CFD)}}{\Delta} - \frac{R_{T(EFD)}}{\Delta}\right)}{\frac{R_{T(EFD)}}{\Delta}} \times 100\% \tag{12}$$

$$RSME = \sqrt{\sum_{i=1}^{N} \frac{\left(E_\%{}^2\right)}{N}} \tag{13}$$

3.2 Total Resistance Investigation

The values measured as the foundation for investigation encompass both the overall resistance and the individual components of ship resistance across each respective variation, subsequently subjected to comparative analysis. The examination of disparities in total resistance values is elaborated upon within this subsection, while a more detailed discussion regarding the friction resistance and residual resistance components is deferred to the subsequent subsection.

The first method involves comparing all variations to the value of the bare hull using Eq. (14). Meanwhile, the second method entails comparing the predicted values of all variations of the interceptor blade shapes with the original (square-shaped) interceptor blade using Eq. (15). In Eq. (14) and Eq. (15), variable "i" denotes a specific variation, such as ½ V, round, and so forth. Here, "bh" is used to denote the bare hull, and "or" is used to denote the original (square-shaped).

$$\delta_{bh}\%_{(R_T/\Delta)} = \frac{(R_T/\Delta)_i - (R_T/\Delta)_{bh}}{(R_T/\Delta)_{bh}} \times 100\% \tag{14}$$

$$\delta_{or}\%_{(R_T/\Delta)} = \frac{(R_T/\Delta)_i - (R_T/\Delta)_{or}}{(R_T/\Delta)_{or}} \times 100\% \tag{15}$$

The results of the comparison of total resistance values (R_T/Δ) between the bare hull and all variations are presented in Table 6. From the table, it is evident that all variations of interceptor blade shapes are effective in reducing resistance only at low speeds, specifically at Fr 0.74. However, at medium speeds (Fr 0.86), there is an increase in resistance for all interceptor variations, although the increment is relatively small, approximately 1%. At this speed, it can be considered that interceptors with the specified height and width configuration are ineffective. The cause of this lies in the height of the interceptor, set at 10mm, which evidently has a significant impact on the interceptor's performance at certain speeds. Even at a speed of Fr 0.99, all interceptor variations result in a significant increase in resistance, reaching around 20%, indicating that interceptors with the specified height and width are detrimental to this vessel. Indeed, the effectiveness of interceptors is also influenced by the hull shape itself. Furthermore, this patrol boat has a relatively small deadrise angle of 15% and features adequate tunnels in the bottom to accommodate the entry of water for the twin propellers, as shown in Fig. **2**. Those factors are also believed to influence the relative effectiveness of interceptor usage.

Table 6
The comparison of predicted values for total resistance involves utilizing the bare hull as the baseline for comparison, followed by a subsequent comparison with the square-shaped form

Fr	R_T/Δ of Bare Hull	$\delta_{bh}\%_{(R_T/\Delta)}$				$\delta_{or}\%_{(R_T/\Delta)}$		
		Square	1/2 V	Round	Full-V	1/2 V	Round	Full-V
0.74	6.15	-7.94	-6.55	-7.57	-5.97	1.51	0.40	2.14
0.86	6.96	0.32	0.30	0.45	1.73	-0.01	0.13	1.41
0.99	7.71	20.60	20.24	14.91	21.85	-0.29	-4.71	1.04

In this study, the primary focus is indeed on comparing the resistance resulting from variations in the cross-sectional shape of the interceptor blade, as reflected in the results presented in Table 6. Based on the comparison of the percentage change in total resistance values $\delta_{or}\%_{(R_T/\Delta)}$, it can be observed that at a speed of Fr 0.74, the square shape performs better and is relatively similar to the round shape. At Fr 0.86, the ½ V shape is slightly more effective than the square (original). Furthermore, at Fr 0.99, the round shape outperforms the square by almost 5%, while the ½ V shape is only 0.3% better than the square. Overall, the round shape exhibits a more stable effectiveness or is nearly suitable under all conditions. Why these shape differences result in differences in total resistance needs to be broken down to see how they affect the components of friction and pressure resistance, where pressure resistance here is represented by the residual resistance of the boat.

3.3 Frictional Resistance Investigation

To delve deeper into understanding the impact of the interceptor on changes in ship resistance, it is essential to dissect the alterations in each resistance component. For fast ships, the resistance components can be conveniently analyzed by concentrating solely on frictional resistance and residuary resistance. This approach is favored because predicting frictional resistance, viscous pressure, and wave-making resistance can be challenging due to the variable form factor of fast-planing craft. Therefore, in this study, we only consider frictional resistance and residuary resistance as the discussed resistance components, with their equations detailed in Eq. (16).

$$R_T = R_F + R_R \tag{16}$$

Similar to how the total resistance results were compared in the previous section, the comparison of frictional resistance for each variation is conducted in a similar manner. Eq. (17) outlines the method for comparing the differences in frictional resistance for each variation with the bare hull value. Subsequently, Eq. (18) is used to compare the effectiveness of the other interceptor blade shapes by comparing each variation with the square shape (original). Then, all these values are summarized in Table 7.

$$\delta_{bh}\%_{(R_F/\Delta)} = \frac{(R_F/\Delta)_i - (R_F/\Delta)_{bh}}{(R_F/\Delta)_{bh}} \times 100\% \tag{17}$$

$$\delta_{or}\%_{(R_F/\Delta)} = \frac{(R_F/\Delta)_i - (R_F/\Delta)_{or}}{(R_F/\Delta)_{or}} \times 100\% \tag{18}$$

Table 7
The comparison of predicted values for frictional resistance involves utilizing the bare hull as the baseline for comparison, followed by a subsequent comparison with the square-shaped form

Fr	R_F/Δ of Bare Hull	$\delta_{bh}\%_{(R_F/\Delta)}$				$\delta_{or}\%_{(R_F/\Delta)}$		
		Square	1/2 V	Round	Full-V	1/2 V	Round	Full-V
0.74	0.99	4.02	6.11	0.89	6.46	2.01	-3.01	2.34
0.86	1.27	13.99	15.77	15.85	16.16	1.56	1.63	1.90
0.99	1.51	41.36	42.11	31.91	42.08	0.53	-6.69	0.51

The results of the comparison of frictional resistance values (R_F/Δ) between the bare hull and all variations are presented in Table 7. From the table, it can be observed that all variations of the interceptor blade shapes actually increase frictional resistance. At Fr 0.74, only the round-shaped interceptor blade slightly increases its frictional resistance, around 1%, while the others range from 4% to 6%. Then, at Fr 0.86, all variations of the interceptor blade shapes result in an increase in frictional resistance ranging from 14% to 16%. At Fr 0.99, all variations of the interceptor blade shapes increase frictional resistance from 32% to 42%. When compared among the installed interceptors, the round-shaped interceptor blade exhibits the lowest frictional resistance.

The increase in frictional resistance occurs due to the installation of interceptors, causing a change in the trim of the hull. As depicted in Fig. **8**, with the installation of interceptor blades, the hull's trim appears smaller than that of the bare hull. From this observation, it is evident that such trim causes the immersed area of the hull to be larger, resulting in higher frictional resistance. The installation of interceptors leads to a smaller trim of the hull compared to without interceptors, expanding the wetted surface area of the hull and causing an increase in frictional resistance. However, the total resistance may paradoxically decrease at times. This implies that there are changes in other resistance components, which will be discussed in the following sections.

(a)

(b)

(c)

(d)

(e)
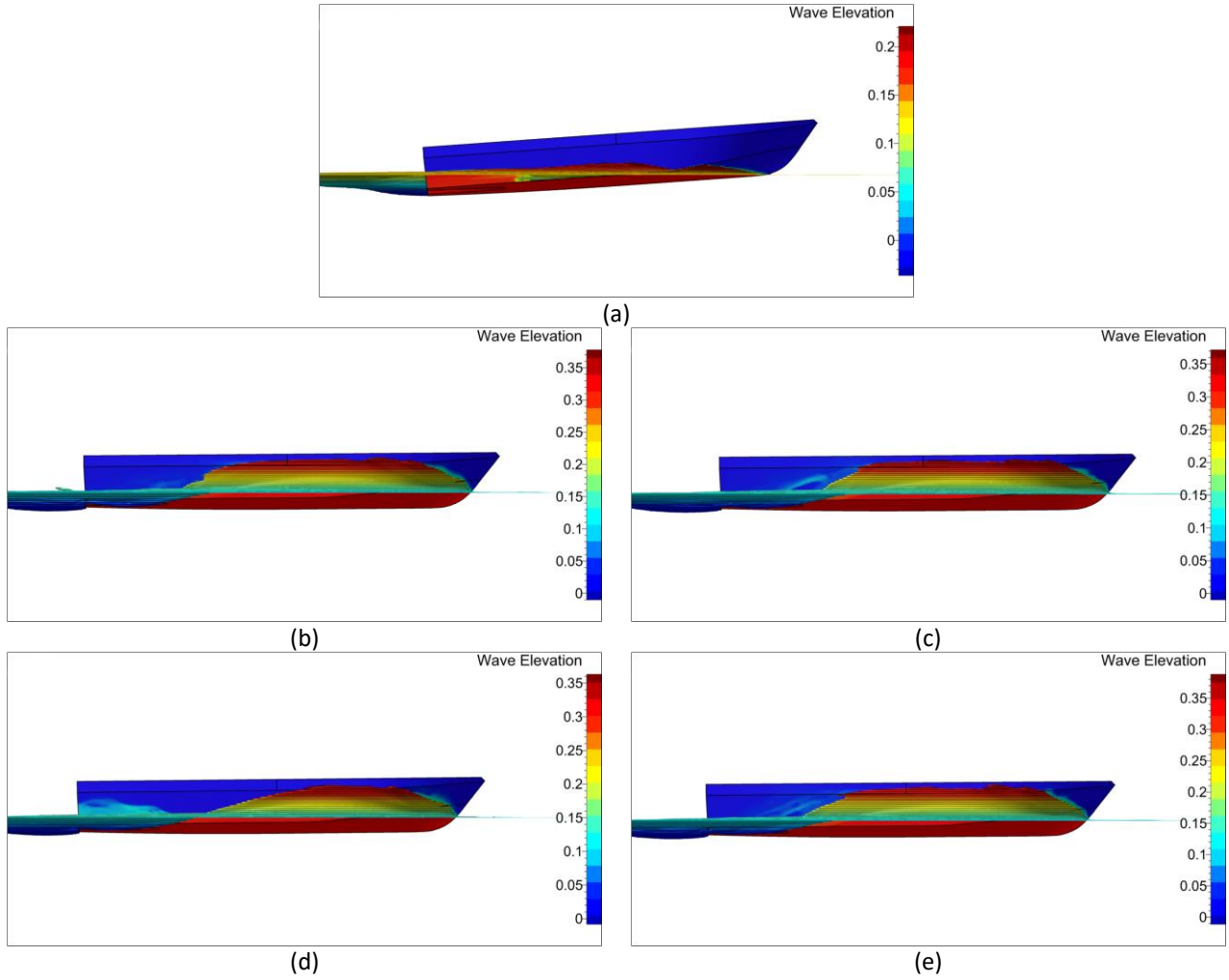
Fig. 8. The influence of the interceptor causing changes in trim and wetted surface area at Fr 0.99: (a) bare hull; interceptor blades (b) Square shape (c) ½ V, (d) round, (e) full-V

3.4 Residual Resistance Investigation

After discussing total resistance and friction, this section finally addresses the residual resistance that occurs due to the installation of interceptors and its variations in the shape of the interceptor blades. Similar to the previous method, the comparison is made using the same equations but specifically for residual resistance, as shown in Eq. (19) and Eq. (20). The results of the comparison are organized in Table 8. Several plots supporting the results of the residual resistance comparison are explained in Fig. **9** as dynamic pressure distribution and Fig. **10** as a comparison of the formed wave patterns.

$$\delta_{bh}\%_{(R_R/\Delta)} = \frac{(R_R/\Delta)_i - (R_R/\Delta)_{bh}}{(R_R/\Delta)_{bh}} \times 100\% \tag{19}$$

$$\delta_{or}\%_{(R_R/\Delta)} = \frac{(R_R/\Delta)_i - (R_R/\Delta)_{or}}{(R_R/\Delta)_{or}} \times 100\% \tag{20}$$
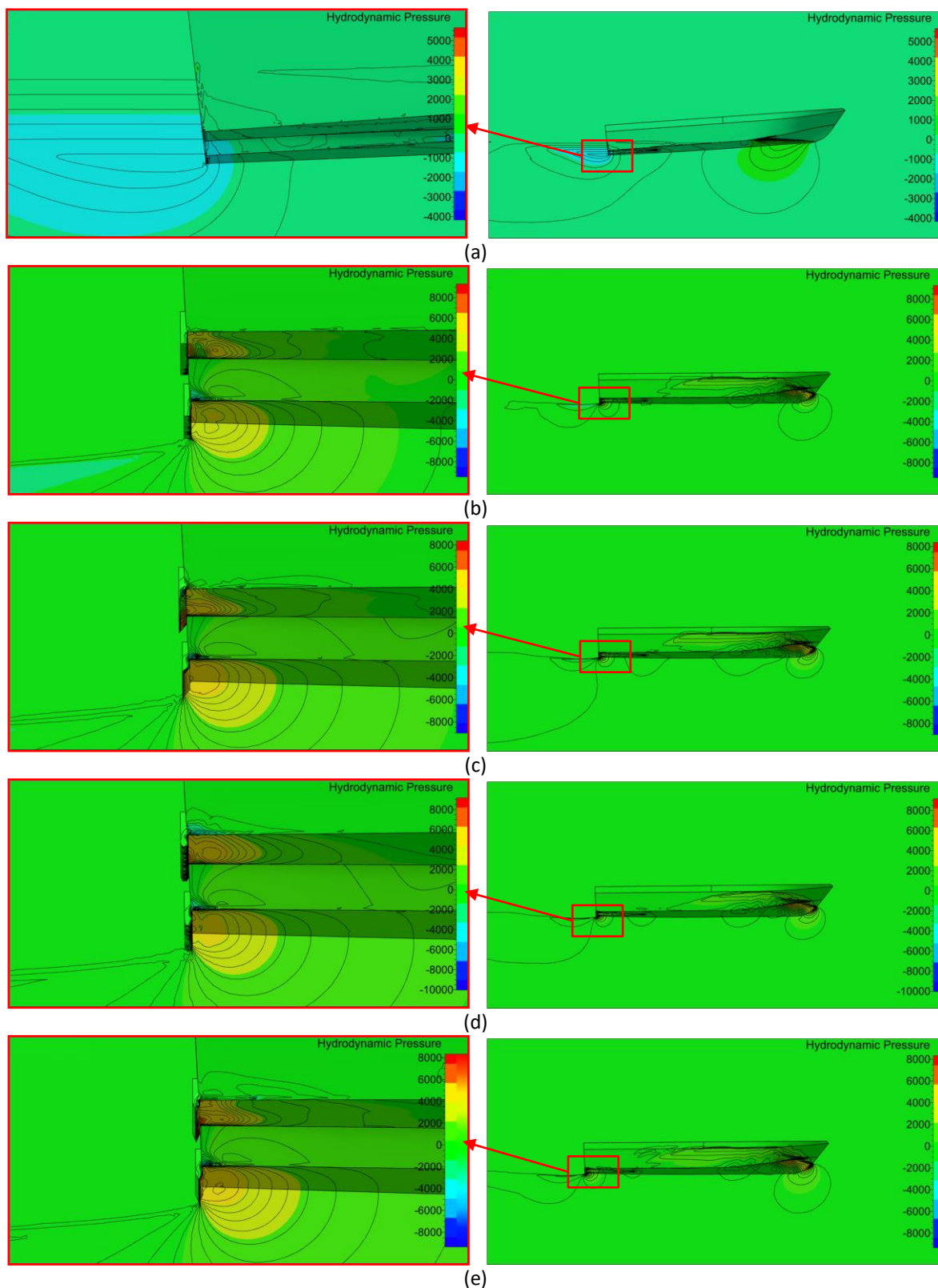
Fig. 9. Comparison of dynamic pressure (a) bare hull; interceptor blades (b) square shape (c) ½ V (d) round (e) full-V

The comparison of residual resistance due to the installation of various forms of interceptor blades is explained in Table 8. Based on the data, it can be seen that at Fr 0.74, the installation of interceptors can significantly reduce residual resistance, ranging from 8% to 10%, with the square

(original) shape being the most effective. Then, at Fr 0.86, all interceptors can still reduce residual resistance, but to a very small extent, around 1-3%. Unfortunately, at high speeds corresponding to Fr 0.99, all forms of interceptors actually increase residual resistance by up to 17%, with the round shape resulting in the smallest increment.

Table 8
The comparison of predicted values for residual resistance involves utilizing the bare hull as the baseline for comparison, followed by a subsequent comparison with the square-shaped form

Fr	R_R/Δ of Bare Hull	$\delta_{bh}\%$				$\delta_{or}\%$		
		Square	1/2 V	Round	Full-V	1/2 V	Round	Full-V
0.74	5.16	-10.24	-8.98	-9.20	-8.36	6.30	5.21	9.41
0.86	5.69	-2.75	-3.16	-3.01	-1.50	-1.63	-1.02	4.88
0.99	6.20	15.53	14.91	10.77	16.92	-1.80	-13.83	4.01

(a)

(b)

(c)

(d)

(e)
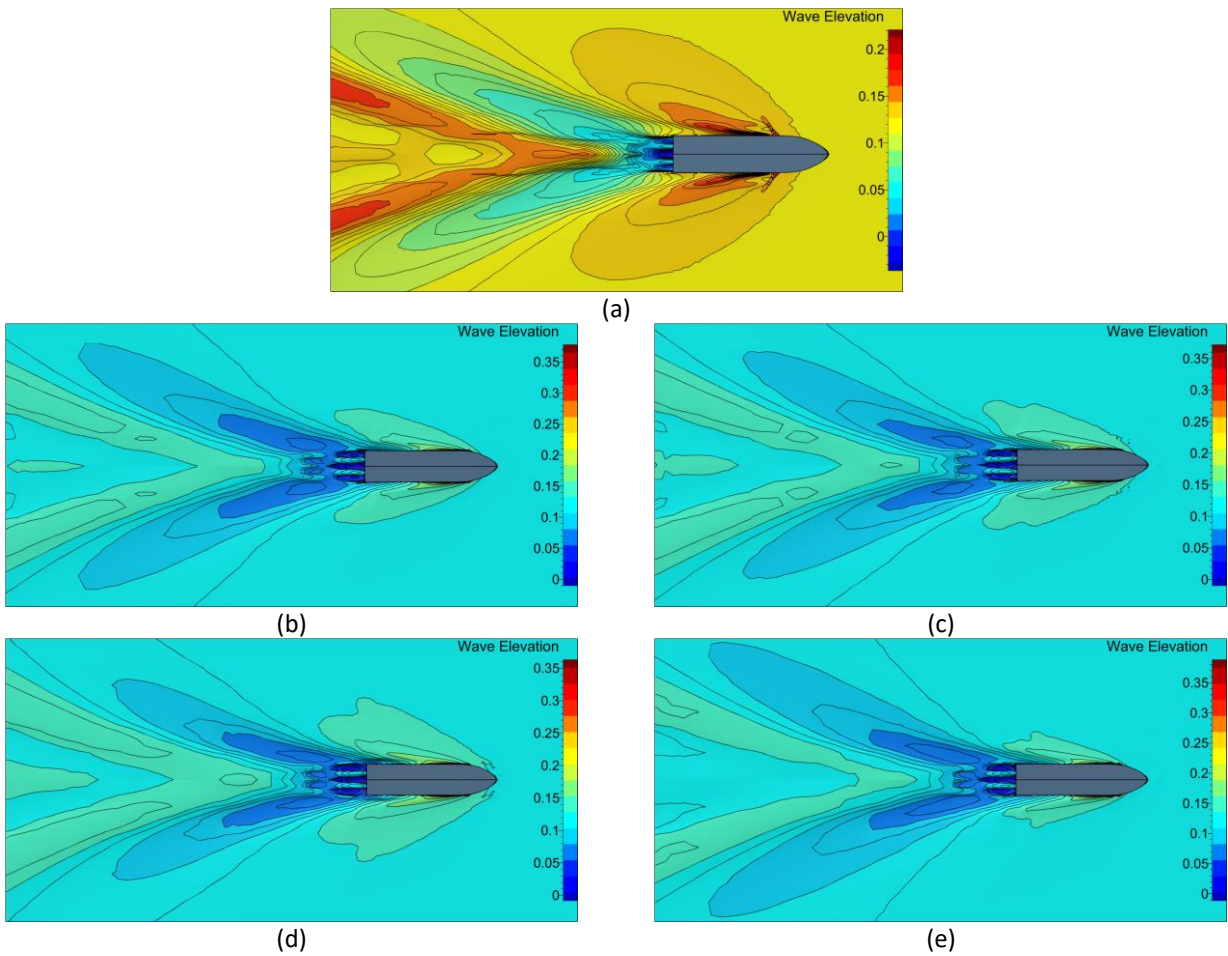
Fig. 10. Differences in wave elevation and form at Fr 0.99 (a) bare hull; interceptor blades (b) square shape (c) ½ V (d) round (e) full-V

Fig. **9** and Fig. **10** provide supporting explanations for the differences in residual resistance results due to the installation of interceptors and various forms of interceptor blades. As explained in Fig. **9**, the installation of interceptors causes a change in pressure distribution, resulting in a corresponding change in wave resistance. Referring back to Fig. **8**, when the hull experiences excessive stern trim, as seen in the bare hull, the wake generated behind the transom is very high, leading to high wave resistance. With the installation of interceptors, the trim of the hull returns to normal, reducing the

wake formed behind the transom and consequently decreasing residual resistance. However, this reduction comes at the expense of higher frictional resistance due to the increased wetted surface area resulting from the reduced trim.

4. Conclusions

An investigation has been conducted on variations in the cross-sectional shape of interceptor blades installed on a high-speed planing boat, where resistance values were predicted using the CFD method that has been well-verified and validated. The tested variations include the commonly used square shape (original) and modifications with other shapes such as ½ V, round, and full-V. The investigation aimed to determine the most effective shape by comparing the total resistance, frictional resistance, and residual resistance values.

From the CFD simulation results for various shapes of interceptor blades, it is found that the round shape is the most favorable. "The most favorable" here refers to producing consistently lower resistance at all speeds comparing rectangular, ½ V, and full V shapes. Similarly, regarding the friction and residual resistance components, the round shape is relatively superior at all speeds. At its highest, the round shape is 4.7% better than the rectangular (original) shape. This research also reveals that the effectiveness of the interceptor is influenced by the hull shape, indicating that different hull shapes and speed selections will require different interceptor design configurations. Therefore, further research with more complex variations is warranted.

Reference
[1]   Doctors, Lawrence J. *Hydrodynamics of high-speed small craft*. No. 292. 1985.
[2]   Faltinsen, Odd M. *Hydrodynamics of high-speed marine vehicles*. Cambridge university press, 2005.
[3]   Hakim, Muhammad Luqman, Tuswan Tuswan, Ahmad Firdaus, and Ocid Mursid. "Investigating the comparison of ship resistance components between u and v-shaped hulls." *Jurnal Teknologi* 85, no. 3 (2023): 153-164. https://doi.org/10.11113/jurnalteknologi.v85.19382.
[4]   Taunton, D. J., D. A. Hudson, and R. A. Shenoi. "Characteristics of a series of high speed hard chine planing hulls-part 1: performance in calm water." *International Journal of Small Craft Technology* 152 (2010): 55-75. https://doi.org/10.3940/rina.ijsct.2010.b2.96.
[5]   Trimulyono, Andi, Muhammad Luqman Hakim, Chairizal Ardhan, Syaiful Tambah Putra Ahmad, Tuswan Tuswan, and Ari Wibawa Budi Santosa. "Analysis of the double steps position effect on planing hull performances." *Brodogradnja: An International Journal of Naval Architecture and Ocean Engineering for Research and Development* 74, no. 4 (2023): 41-72. https://doi.org/10.21278/brod74403.
[6]   Park, Kyurin, Dong Jin Kim, Sun Young Kim, Jeonghwa Seo, Innduk Suh, and Shin Hyung Rhee. "Effect of waterjet intake plane shape on course-keeping stability of a planing boat." *International Journal of Naval Architecture and Ocean Engineering* 13 (2021): 585-598. https://doi.org/10.1016/j.ijnaoe.2021.06.008.

[7]   Firdhaus, Ahmad, Parlindungan Manik, and Muhammad Luqman Hakim. "CFD Analysis of the Influence of Marine Fouling on the Performance of High-Speed Planning Craft." *Journal of Advanced Research in Fluid Mechanics and Thermal Sciences* 110, no. 2 (2023): 124-137. https://doi.org/10.37934/arfmts.110.2.124137.

[8]   Amiruddin, Wilma, Muhammad Luqman Hakim, Ahmad Firdhaus, Dian Purnamasari, Tuswan Tuswan, Samuel Samuel, and Ocid Mursid. "Prediction of the impact of biofouling roughness on a full-scale planing boat performance using CFD." *Ocean Engineering* 301 (2024): 117457. https://doi.org/10.1016/j.oceaneng.2024.117457.

[9]   Hakim, Muhammad Luqman, Bagus Nugroho, Rey Cheng Chin, Teguh Putranto, I. Ketut Suastika, and I. Ketut Aria Pria Utama. "Drag penalty causing from the roughness of recently cleaned and painted ship hull using RANS CFD." *CFD Letters* 12, no. 3 (2020): 78-88. https://doi.org/10.37934/cfdl.12.3.7888.

[10]   Hakim, Muhammad Luqman, Niko Maqbulyani, Bagus Nugroho, I. Ketut Suastika, and I. K. A. P. Utama. "Wind-tunnel experiments and CFD simulations to study the increase in ship resistance components due to roughness." *Journal of sustainability science and management* 16, no. 3 (2021): 144-163. https://doi.org/10.46754/jssm.2021.04.012.

[11]   Hakim, Muhammad Luqman, Bagus Nugroho, I. Ketut Suastika, and I. K. A. P. Utama. "Alternative empirical formula for predicting the frictional drag penalty due to fouling on the ship hull using the design of experiments (doe) method." *International Journal of Technology* 12, no. 4 (2021): 829. https://doi.org/10.14716/ijtech.v12i4.4692.

[12]   Hakim, Muhammad Luqman, Dian Purnamasari, Muryadin Muryadin, Fariz Maulana Noor, Putri Virliani, Endah Suwarni, Rina Rina, Nurcholis Nurcholis, and Rio Dwi Sakti Wijaya. "Using trim Control to Improve energy Efficiency on High-Speed Marine Vehicles (HSMV): A Review." (2023): 1603-1615. https://doi.org/10.5109/7151709.

[13]   Samuel, S., Ocid Mursid, Serliana Yulianti, Kiryanto Kiryanto, and Muhammad Iqbal. "Evaluation of interceptor design to reduce drag on planing hull." *Brodogradnja: An International Journal of Naval Architecture and Ocean Engineering for Research and Development* 73, no. 3 (2022): 93-110. https://doi.org/10.21278/brod73306.

[14]   Mansoori, M., A. C. Fernandes, and H. Ghassemi. "Interceptor design for optimum trim control and minimum resistance of planing boats." *Applied Ocean Research* 69 (2017): 100-115. https://doi.org/10.1016/j.apor.2017.10.006.

[15]   Fitriadhy, Ahmad, Loke Yan Pheng, Iqmal Nor Hakim Adzkh, Faisal Mahmuddin, Anuar Abu Bakar, Mohd Azlan Musa, and Mohd Sofiyan Sulaiman. "Computational investigation of pitch motion of a high-speed craft incorporated with trim-tabs." *CFD Letters* 14, no. 6 (2022): 56-71. https://doi.org/10.37934/cfdl.14.6.5671.

[16]   Ghadimi, Parviz, Afshin Loni, Hashem Nowruzi, Abbas Dashtimanesh, and Sasan Tavakoli. "Parametric study of the effects of trim tabs on running trim and resistance of planing hulls." *Advances in shipping and Ocean Engineering* 3, no. 1 (2014): 1-12.

[17]   Syahrudin, Muhamad Fuad, Muhammad Arif Budiyanto, and Muhammad Aziz Murdianto. "Analysis of the use of stern foil on the high speed patrol boat on full draft condition." (2020): 262-267. https://doi.org/10.5109/4055230.

[18]   Samuel, Andi Trimulyono, Parlindungan Manik, and Deddy Chrismianto. "A numerical study of spray strips analysis on fridsma hull form." *Fluids* 6, no. 11 (2021): 420. https://doi.org/10.3390/fluids6110420.

[19]   Lakatoš, Mikloš, Kristjan Tabri, Abbas Dashtimanesh, and Henrik Andreasson. "Numerical Modelling of a Planing Craft with a V-Shaped Spray Interceptor Arrangement in Calm Water." In *HSMV 2020*, pp. 33-42. IOS Press, 2020. https://doi.org/10.3233/PMST200024.

[20] Lakatoš, Mikloš, Tarmo Sahk, Henrik Andreasson, and Kristjan Tabri. "The effect of spray rails, chine strips and V-shaped spray interceptors on the performance of low planing high-speed craft in calm water." *Applied Ocean Research* 122 (2022): 103131. https://doi.org/10.1016/j.apor.2022.103131.

[21] Karimi, Mohammad Hosein, Mohammad Saeed Seif, and Madjid Abbaspoor. "An experimental study of interceptor's effectiveness on hydrodynamic performance of high-speed planing crafts." *Polish maritime research* 20, no. 2 (2013): 21-29. https://doi.org/10.2478/pomr-2013-0013.

[22] Deng, R., S. Y. Chen, T. C. Wu, F. Q. Luo, D. P. Jiang, and Y. L. Li. "Investigation on the influence induced by interceptor on the viscous flow field of deep-Vee vessel." *Ocean Engineering* 196 (2020): 106735. https://doi.org/10.1016/j.oceaneng.2019.106735.

[23] Jangam, Suneela. "CFD based prediction on hydrodynamic effects of Interceptor and flap combination on planing hull." *Ocean Engineering* 264 (2022): 112523. https://doi.org/10.1016/j.oceaneng.2022.112523.

[24] Batchelor, G. K., and A. D. Young. "An Introduction to Fluid Mechanics." *Journal of Applied Mechanics* 35, no. 3 (September 1, 1968): 624–624. https://doi.org/10.1115/1.3601282.

[25] Ferziger, Joel H., and Milovan Perić. *Computational methods for fluid dynamics*. New York: Springer, 2002. https://doi.org/10.1007/978-3-642-56026-2.

[26] Hirt, Cyril W., and Billy D. Nichols. "Volume of fluid (VOF) method for the dynamics of free boundaries." *Journal of computational physics* 39, no. 1 (1981): 201-225. https://doi.org/10.1016/0021-9991(81)90145-5.

[27] Menter, Florian R. "Two-equation eddy-viscosity turbulence models for engineering applications." *AIAA journal* 32, no. 8 (1994): 1598-1605. https://doi.org/10.2514/3.12149.

[28] ITTC. "ITTC – Recommended Procedures and Guidelines - Practical Guidelines for Ship CFD Applications. 7.5-03-02-03 (Revision 01)." *ITTC – Recommended Procedures and Guidelines*, 2014.

[29] Matveev, Konstantin I. "Two-dimensional modeling of stepped planing hulls with open and pressurized air cavities." *International Journal of Naval Architecture and Ocean Engineering* 4, no. 2 (2012): 162-171. https://doi.org/10.2478/IJNAOE-2013-0087.